

Study of Configuration Differentia and Highly Efficient, Deep-Blue, Organic Light-Emitting Diodes Based on Novel Naphtho[1,2-*d*]imidazole Derivatives

Ming Liu, Xiang-Long Li, Dong Cheng Chen, Zhongzhi Xie, Xinyi Cai, Gaozhan Xie, Kunkun Liu, Jianxin Tang, Shi-Jian Su,* and Yong Cao

Two novel naphtho[1,2-*d*]imidazole derivatives are developed as deep-blue, light-emitting materials for organic light-emitting diodes (OLEDs). The 1*H*-naphtho[1,2-*d*]imidazole based compounds exhibit a significantly superior performance than the 3*H*-naphtho[1,2-*d*]imidazole analogues in the single-layer devices. This is because they have a much higher capacity for direct electron-injection from the cathode compared to their isomeric counterparts resulting in a ground-breaking EQE (external quantum efficiency) of 4.37% and a low turn-on voltage of 2.7 V, and this is hitherto the best performance for a non-doped single-layer fluorescent OLED. Multi-layer devices consisting of both hole- and electron-transporting layers, result in identically excellent performances with EQE values of 4.12–6.08% and deep-blue light emission (Commission Internationale de l'Éclairage (CIE) γ values of 0.077–0.115) is obtained for both isomers due to the improved carrier injection and confinement within the emissive layer. In addition, they showed a significantly better blue-color purity than analogous molecules based on benzimidazole or phenanthro[9,10-*d*]imidazole segments.

1. Introduction

Organic light-emitting diodes (OLEDs) have attracted considerable attention owing to their potential applications in both new generation full-color flat-panel displays and solid-state lighting.^[1] During the past two decades, numerous efforts have been devoted to developing new OLED emitters, and great success has been achieved, particularly for heavy metal complex phosphorescent emitters.^[2] However, because of the difficulty

in obtaining wide energy-gap phosphors, reports regarding highly efficient blue phosphors that exhibit deep-blue emission with Commission Internationale de l'Éclairage (CIE) γ values smaller than 0.15 are exiguous, and their short device lifetimes are not suitable for commercial applications. Adachi et al. developed deep-blue OLEDs based on thermally activated delayed fluorescence (TADF) with CIE coordinates of (0.15, 0.07) and a high EQE of 9.9% at low current density.^[3] However, in this type of device, the serious roll-off in efficiency will have to be solved. Moreover, deep-blue phosphorescent and TADF devices require host and periphery materials with a high enough triplet energy to confine the triplet excitons on the emitter, which remains a challenge.^[4] To address these issues, investigators keep focusing their work on conventional blue fluorophores, in which stability and high color

purity can be readily realized.^[3,5] Furthermore, non-doped fluorescent devices can play a crucial role in reducing the cost of production and simplifying the manufacturing process of full-color displays and white-light sources. Yet, most of the reported devices with non-doped emitting layers have been shown to have an unimpressive external quantum efficiency (EQE) or insufficient deep-blue emission.^[6] Particularly, for simplified single-layer devices, which are greatly in favor to limit the overall cost, reports in which the devices have an EQE of 3% or higher are rare.^[7] Therefore, developing highly efficient, blue, fluorescent materials remain a significant challenge.

There are several prerequisites for high-performance fluorescent OLEDs with a non-doped light-emitting layer: 1) fluorescent molecules with high fluorescent quantum yields; 2) a good balance between electron and hole injection as well as localizing the carrier-recombination region in the light-emitting layer; 3) appropriate energy levels of light-emitting molecules, which match to that of the periphery layers or electrodes; 4) good film-forming property and morphological stability of the organic materials. Generally, unbalanced carrier injection and transportation induces an increase in the driving voltage and a decrease in the device efficiency. Therefore, ambipolar molecules with a donor-acceptor (D-A) structure that encourages the balance of carrier transport are desirable candidates for high-efficiency OLEDs with non-doped emitting layers. On the other hand, D-A

M. Liu, X. L. Li, D. C. Chen, X. Y. Cai, G. Z. Xie,
K. K. Liu, Prof. S.-J. Su, Prof. Y. Cao
State Key Laboratory of Luminescent
Materials and Devices
Institute of Polymer Optoelectronic
Materials and Devices
South China University of Technology
Guangzhou 510640, P. R. China
E-mail: mssjsu@scut.edu.cn

Z. Z. Xie, Prof. J. X. Tang
Jiangsu Key Laboratory for Carbon-Based
Functional Materials & Devices
Institute of Functional Nano & Soft Materials (FUNSOM)
Soochow University
Suzhou 215123, P. R. China



DOI: 10.1002/adfm.201502163

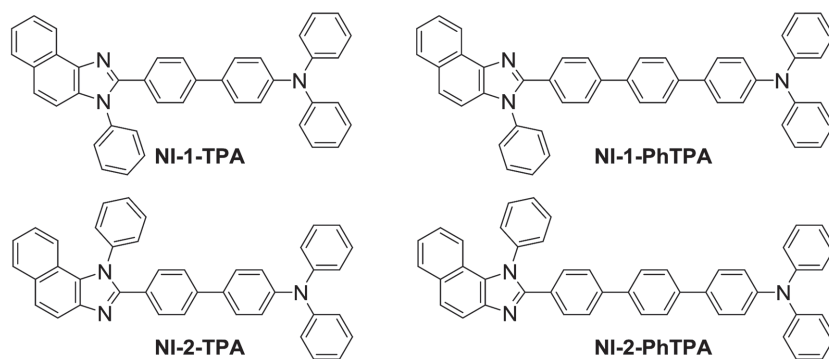


Figure 1. Molecular structures of the naphtho[1,2-*d*]imidazole derived compounds NI-1-TPA, NI-2-TPA, NI-1-PhTPA, and NI-2-PhTPA.

molecular systems are liable to cause extended π -conjugation and to generate intramolecular charge transfer (ICT), which gives rise to a bathochromic shift and color impurity of the emission. Therefore, it is clear that controlling the ICT effect to an extent is a prerequisite for deep-blue emission.^[5c] Thus, introducing weak electron-deficient as well as electron-rich segments to prevent bathochromic shift of the emission and simultaneously achieving appropriate energy levels for balanced electron and hole injection has been regarded as an advisable strategy for designing D–A type, deep-blue, light-emitting compounds. In recent years, an increasing amount of blue light-emitting compounds containing imidazole derivatives, for instance, benzimidazole (BI) and phenanthro[9,10-*d*]imidazole (PI), as the electron-deficient component has been reported with high device efficiency.^[5b,8] The predominant result of these investigations demonstrates that imidazole derivatives can serve as preeminent electron-withdrawing components for the construction of promising blue-light-emitting molecules. The electron-deficiency properties of imidazole derivatives are usually weak to avoid problems with ICT and the resulting red shift of the emission spectra. These advantages have made imidazole, BI, and PI some of the most commonly used segments for organic electroluminescent materials in recent years.^[9]

Herein, we report on two naphtho[1,2-*d*]imidazole (NI) isomers, namely, 3*H*-naphtho[1,2-*d*]imidazole (NI-1) and 1*H*-naphtho[1,2-*d*]imidazole (NI-2), and a series of their derivatives, which were designed and synthesized as highly efficient, blue-fluorescent emitters for non-doped single- and multi-layer electroluminescent devices. Interestingly, our single-layer devices based on NI-1 molecules displayed an inferior efficiency and distinctly higher driving voltage than the devices based on NI-2. The reasons for this phenomenon will be discussed hereafter. However, in our multi-layer devices, all of the blue fluorophores exhibited a high EQE, indicating their efficacy as non-doped blue emitters. Moreover, our study also discovered that the NI compounds have an advantage over the BI and PI analogues in their blue-color purity.

2. Results and Discussions

2.1. Molecular Design, Synthesis, and Theoretical Calculations

These fluorophores adopt triphenylamine (TPA), a generally used hole-transporting unit, as the electron-rich group,^[10] and

different numbers of benzene rings between the NI unit and TPA could play a role in tuning the conjugation length. The molecular structures of our new compounds, NI-1-TPA, NI-2-TPA, NI-1-PhTPA, and NI-2-PhTPA, are shown in **Figure 1**, and their synthetic routes are outlined in **Scheme 1**. The pivotal precursors NI-1-Br and NI-2-Br were synthesized from 1-nitro-2-naphthol and 2-nitro-1-naphthol, respectively, through five steps with considerable yields. Finally, reactions of NI-1-Br or NI-2-Br with *N,N*-diphenyl-4-(4,4,5,5-tetramethyl-1,3,2-dioxaborolan-2-yl)aniline or *N,N*-diphenyl-4'-(4,4,5,5-tetramethyl-1,3,2-dioxaborolan-2-yl)-[1,1'-biphenyl]-4-amine were carried out by a palladium-catalyzed

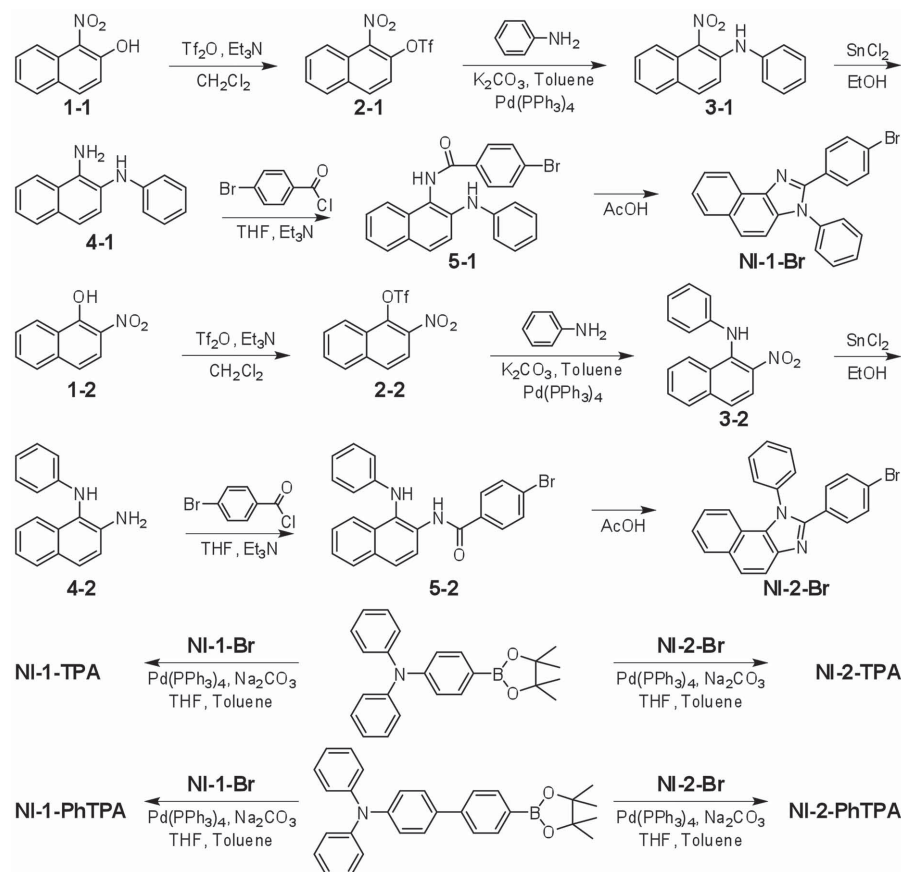
Suzuki cross-coupling reaction to give NI-1-TPA, NI-2-TPA, NI-1-PhTPA, and NI-2-PhTPA. All products were fully characterized by ¹H, ¹³C NMR spectrometry, mass spectrometry, and elemental analysis. To evaluate their frontier molecular orbitals and energy bandgaps, density functional theory (DFT) calculations were performed with a B3LYP/6–31G(d,p) basis set using the Gaussian 03W program (Figure S1 and Table S1 in the Supporting Information).^[11] Although these four compounds are different in conjugation length and/or configuration of the naphtho[1,2-*d*]imidazole units, their calculated lowest unoccupied molecular orbitals (LUMOs) and highest occupied molecular orbitals (HOMOs) were quite similar. But on the basis of theoretical calculations, the NI-1 based compounds were predicted to exhibit a slightly narrower energy bandgap (E_g) and smaller singlet excited energy (S_1) than their NI-2 isomeric counterparts.

2.2. Thermal, Electrochemical, and Optical Properties

All compounds showed good thermal stability, which is indicated by their high decomposition temperatures (T_d , corresponding to 5% weight loss) ranging between 372.2 and 400.5 °C, as obtained from thermogravimetric analyses (TGA) and their glass-transition temperatures (T_g) of 113.8, 110.2, 127.1, and 124.2 °C for NI-1-TPA, NI-2-TPA, NI-1-PhTPA, and NI-2-PhTPA, respectively, as determined from differential scanning calorimetry (DSC) (Figure S2, Supporting Information). The NI-1 compounds exhibited a slightly higher T_g than their NI-2 analogues, but the thermal properties of all four compounds were good enough for application in electroluminescent devices.

Cyclic voltammetry (CV) was used to measure their ionization potentials (IPs). Each compound displayed a reversible oxidation wave, which could be attributed to the oxidation of the arylamine units (Figure S3, Supporting Information). The IPs of these NI compounds were calculated from the onset oxidation potential (E_{ox} vs ferrocene/ferricenium) and found to be almost the same (about -5.22 ± 0.01 eV), despite their differences in configuration and/or conjugation length.^[12]

The photophysical data are collected in **Table 1**, and representative UV-vis absorption and photoluminescence (PL) spectra are shown in Figure S4 (Supporting Information). The absorption



Scheme 1. Synthetic routes for the naphtho[1,2-*d*]imidazole derived compounds NI-1-TPA, NI-2-TPA, NI-1-PhTPA, and NI-2-PhTPA.

spectra of all four NI molecules in the thin-film state show an obviously broader peak and slight red-shift of the peak compared to the absorption spectra of the NI molecules in DCM solution. These phenomena imply that the emitters reported herein form a compact stacking structure in the thin film that benefits charge transport. The NI-2 based compounds NI-2-TPA and NI-2-PhTPA display a subtle hypsochromic shift compared to their isomeric counterparts, which is consistent with theoretical calculations. All of our compounds were highly emissive in the blue region with peaks in the range of 445–448 nm. According to the onset of the absorption in the thin film, the optical energy bandgaps (E_g^{opt}) of NI-1-TPA, NI-2-TPA, NI-1-PhTPA, and NI-2-PhTPA were determined to be 2.89, 2.92, 2.86, and 2.89 eV, respectively. We failed to obtain the reduction potential of these compounds from the CV measurements, and thus their electron affinities (EAs) were estimated from their IP and E_g^{opt} values to be -2.32 , -2.30 , -2.36 , and -2.34 eV, respectively.

Their PL and UV-vis absorption spectra were also studied in various solvents, as shown in Figure S5, and the data are summarized in Table S2, both in the Supporting Information. Insignificant changes were found in their absorption spectra with increasing solvent polarity, indicating a negligible dipolar change at the ground state in different solvents. However, their fluorescence spectra were rather broadened and gradually shifted bathochromically by increasing the polarity of the solvent, which implies a large increased transition of the dipole

moment from the ground state to the excited state. We also plotted the Stokes shift versus the orientation polarizability (f), as shown in Figure S6 (Supporting Information). Two distinguishable excited states in high- and low-polarity solvents were found. According to the investigations by Ma and colleagues, the current naphtho[1,2-*d*]imidazole compounds may also possess a totally intercrossed excited state of the local exciton (LE) and charge transfer (CT) (namely hybridized local charge transfer, HLCT) in moderately polar solvents ($0.1 \leq f \leq 0.2$), such as chloroform.^[8c,13] The spectral characteristics of our compounds in the thin-film state were similar to those of their solutions in chloroform. From this it can be inferred that the solid state (the main form for applications) has a similar polarity effect on these NI molecules as that of chloroform, in which they have been assumed to possess an intercrossed excited state. This will be helpful for achieving fluorophores with higher photoluminescence quantum yields (PLQYs) and standard blue-light emission. Consequently, all the NI molecules reported here showed high PLQY values of above 90% in CH_2Cl_2 and of 57–73% in the neat film state. These characteristics show the potential of these compounds as highly efficient electroluminescent materials.

2.3. Electroluminescent Performances

In order to probe their electroluminescent properties, we fabricated single-layer OLEDs as they are easy to process and

Table 1. Physical properties and calculated energy levels of the compounds.

Compound	T_g/T_d^a [°C]	λ_{abs}^b [nm]	λ_{abs}^c [nm]	λ_{em}^b [nm]	λ_{em}^c [nm]	PLQY ^d	$E_g^{opt\ e}$ [eV]	IP/EA ^f [eV]	HOMO/LUMO ^g [eV]	$E_g^{cal\ g}$ [eV]
NI-1-TPA	113.8/373.0	298, 362	302, 368	452	445	0.92 (0.57)	2.89	-5.21/-2.32	-4.91/-1.28	3.63
NI-2-TPA	110.2/372.2	285, 359	289, 363	448	446	0.93 (0.61)	2.92	-5.22/-2.30	-4.90/-1.22	3.68
NI-1-PhTPA	127.1/392.5	302, 359	303, 366	466	448	0.92 (0.73)	2.86	-5.22/-2.36	-4.92/-1.39	3.53
NI-2-PhTPA	124.2//400.5	290, 357	294, 363	462	445	0.93 (0.70)	2.89	-5.23/-2.34	-4.92/-1.33	3.59

^a)Glass-transition temperature (T_g)/decomposition temperature (T_d) (5% weight loss); ^b)UV-vis absorption and PL bands in dichloromethane solutions at room temperature; ^c)UV-vis absorption and PL peaks in neat thin films; ^d)PL quantum yield (PLQY) of the dichloromethane solutions at room temperature. The values in parentheses are obtained from the neat thin films; ^e)Optical energy bandgap (E_g^{opt}) estimated from the absorption edge in thin films; ^f)Ionization potentials (IPs) determined from cyclic voltammetry and electron affinities (EAs) estimated from IPs and E_g^{opt} s; ^g)HOMO and LUMO energy levels and energy bandgaps (E_g^{cal}) obtained from the DFT calculations with B3LYP/6-31G(d,p) basis set by using Gaussian 03W program.

conductive to low-cost production and we investigated them in a configuration of ITO/ HATCN (5 nm)/ NI compound (80 nm)/ LiF (1 nm)/ Al (devices SA to SD), in which HATCN (hexaazatriphenylenehexacarbonitrile) and LiF were used as buffer layers for the anode and cathode, respectively. The device characteristics are shown in **Table 2** and **Figure 2**. Deep-blue electroluminescence was obtained from these single-layer devices with CIE_y values in the range of 0.068–0.113. But, unexpectedly, the devices based on the NI-1 compounds exhibited an unsatisfactory performance with current efficiencies (CE) of 0.04 and 0.54 cd A⁻¹, corresponding to EQE values of 0.05% and 0.52% for the devices SA and SC, respectively. On the contrary, the NI-2 compounds delivered superior device efficiencies. Especially, the NI-2-PhTPA based device, SD, demonstrated a groundbreaking EQE of 4.37%, a CE of 4.28 cd A⁻¹, and a very low turn-on voltage of 2.7 V. This is hitherto the best performance of a non-doped single-layer fluorescent OLED.

The carrier injection and transport properties of these materials, which can be deduced from single-carrier devices, were essential to understand the great disparity between the efficiencies of the single-layer devices. Devices with a configuration of ITO/ HATCN (5 nm)/ NI compound (80 nm)/ Au for the hole-only devices and ITO/ TmPyPB (1,3,5-tri[(3-pyridyl)-phen-3-yl]benzene) (10 nm)/ NI compound (80 nm)/ LiF (1 nm)/ Al for the electron-only devices were fabricated and characterized. The key factor in balancing the carriers in single-layer devices

was the difference in electron injection ability from the cathode into the emitting layers, which was illustrated by the current density of the electron-only devices, as shown in **Figure 3a**, and depends on the operating voltage of the single-layer electroluminescent devices. It seems that the direct injection of electrons from LiF/Al was much easier into the NI-2 compounds than into the NI-1 ones, even though their LUMO levels were alike. On the other hand, the hole-injection from the anode and the transport in each material appeared to be similar for all four compounds, except for NI-1-TPA, which gave a significantly higher current density in the hole-only device than NI-2-TPA, NI-1-PhTPA, and NI-2-PhTPA (**Figure 3b**). This explains why NI-1-TPA had the worst efficiency in a single-layer OLED, where hole transport is the inherently dominant carrier-transport.

We studied the reason why electrons could be much easier injected from LiF/Al into the NI-2 compounds than into the NI-1 ones by using ultraviolet photoelectron spectroscopy (UPS, **Figure 4**) and X-ray photoelectron spectroscopy (XPS, **Figure S7**, Supporting Information). Information from the in situ UPS measurements revealed that incremental deposition of LiF overlayers caused a shift (0.5 eV) in the vacuum level (VL, determined from the onset of the high binding energy (BE) side) of NI-2-PhTPA, but had almost no effect on that of NI-1-PhTPA. XPS measurements were also performed after each deposition step. **Figure S7** displays the N 1s core level

Table 2. Summary of the electroluminescent data of the single-layer (SA-SD) and multi-layer (MA-MD) devices.

Device	EML	λ_{EL} [nm]	FWHM [nm]	CIE ^a (x,y)	V_{on}^b [V]	CE ^c [cd A ⁻¹]	Power efficiency (PE) ^c [lm W ⁻¹]	EQE ^c [%]
SA	NI-1-TPA	444	58	(0.151, 0.075)	3.5	0.04/0.04/–	0.02/0.02/–	0.05/0.05/–
SB	NI-2-TPA	442	56	(0.151, 0.068)	2.8	1.38/1.18/0.90	1.44/0.98/0.49	1.89/1.62/1.24
SC	NI-1-PhTPA	458	62	(0.144, 0.113)	3.0	0.54/0.32/0.54	0.26/0.22/0.24	0.52/0.31/0.52
SD	NI-2-PhTPA	452	62	(0.146, 0.105)	2.7	4.28/4.26/4.00	4.32/4.07/2.90	4.37/4.35/4.08
MA	NI-1-TPA	450	61	(0.145, 0.087)	2.8	3.33/3.28/3.08	3.48/3.19/2.16	4.12/4.06/3.81
MB	NI-2-TPA	448	59	(0.146, 0.077)	2.7	3.76/3.58/3.01	3.93/3.52/2.20	5.16/4.92/4.13
MC	NI-1-PhTPA	458	66	(0.143, 0.115)	2.7	6.35/6.22/5.70	6.96/6.37/4.91	6.08/5.96/5.46
MD	NI-2-PhTPA	452	62	(0.145, 0.100)	2.6	5.46/5.41/5.09	6.12/5.74/4.45	5.95/5.89/5.54

Abbreviations: λ_{EL} : peak wavelength of the EL spectrum, V_{on} : turn-on voltage, and FWHM: full width at half-maximum; ^a)CIE coordinates measured at 100 cd m⁻²; ^b)Driving voltage at 1 cd m⁻²; ^c)Current efficiency (CE), power efficiency (PE), and external quantum efficiency (EQE) in the order of maximum, then the values at 100 and 1000 cd m⁻².

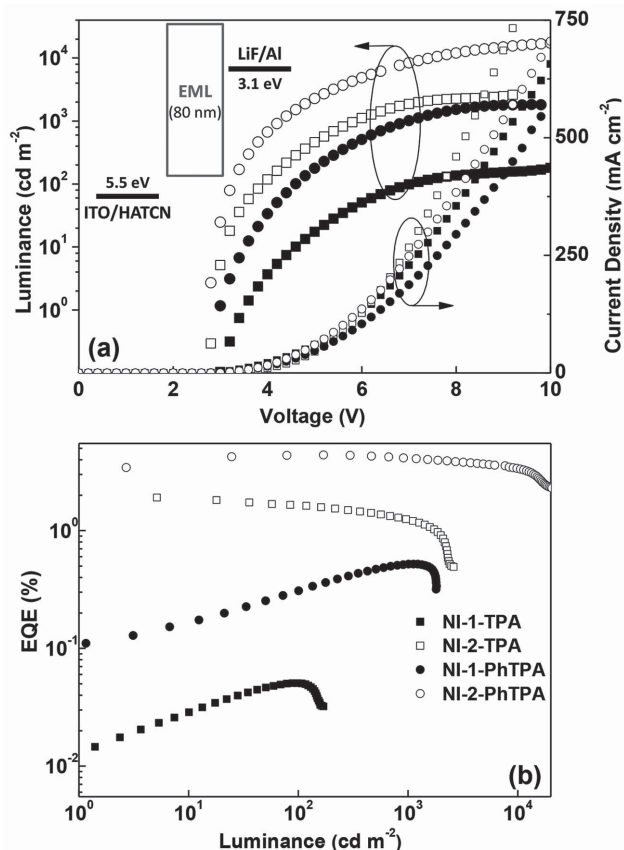


Figure 2. a) Luminance and current density versus voltage and b) EQE versus luminance characteristics for the single-layer devices in a configuration of ITO/ HATCN (5 nm)/ EML (80 nm)/ LiF (1 nm)/ Al. EML: NI-1-TPA, NI-2-TPA, NI-1-PhTPA, or NI-2-PhTPA. Inset: The configuration and energy diagram of the single-layer devices.

spectra of NI-1-PhTPA and NI-2-PhTPA, in which the original peaks around 399.2 eV could be assigned to the chemical state of nitrogen with sp^2 hybridization in accordance to previous research.^[14] The N 1s core level spectra of NI-2-PhTPA shifted slightly toward a higher BE region and became broader, which suggests that a delicate change in the chemical environment has taken place with the gradual deposition of LiF layers. Such changes could not be detected in similar measurements for NI-1-PhTPA. Considering the results from the UPS and XPS

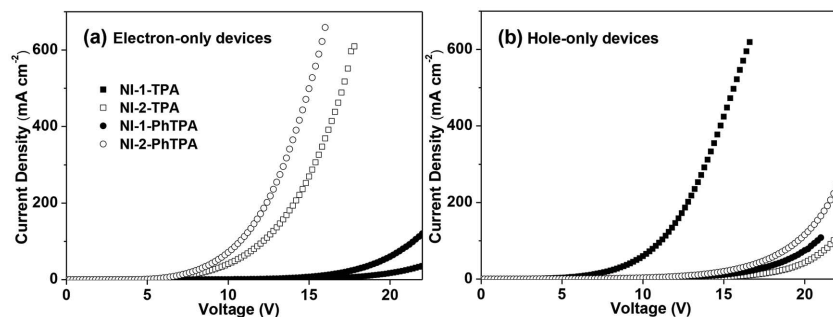


Figure 3. Current density versus voltage characteristics for a) the electron-only devices and b) hole-only devices.

measurements, we suspected that a coordination effect between the exposed nitrogen atom of the NI-2 components and LiF may reduce the energy difference between the interface of the NI-2 compounds and the cathode, resulting in better electron injection and thus a reduced operating voltage. In contrast, the configuration in the NI-1 components may hinder such a coordination which results in a lower electron flux and thus reduced carrier balance for the NI-1 compounds.

In addition, we believe that reducing the charge-injection barrier from the electrodes to the emitting layer will bring about notable progress for the devices based on the NI-1 compounds. To achieve this, OLEDs with multi-layer structures of ITO/ HATCN (5 nm)/ NPB (40 nm)/ TCTA (5 nm)/ NI emitter (20 nm) / TPBI (40 nm)/ LiF (1 nm)/ Al (devices MA-MD) were also fabricated. In these devices, *N,N'*-di-1-naphthyl-*N,N'*-diphenylbenzidine (NPB) and TCTA (4,4',4''-tri(*N*-carbazolyl)-triphenylamine) served as the hole-transporting and electron-blocking layer, respectively, and 1,3,5-tri(phenyl-2-benzimidazolyl)-benzene (TPBI) served as the electron-transporting and hole-blocking layer. The current density–voltage–luminance (J – V – L), EQE, and power efficiency versus luminance characteristics of the multi-layer devices are shown in Figure 5. Because of the improvements in charge injection into the emissive layer and in carrier confinement, the multi-layer devices based on the NI-1 compounds reached the same level of performance as those based on the NI-2 ones. All devices displayed a similarly low turn-on voltages in the range of 2.6–2.8 V thanks to the small carrier injection barrier. The devices MA and MB, based on the molecules NI-1-TPA and NI-2-TPA that both have a shorter conjugation length, exhibit deep blue emissions with CIE coordinates of (0.145, 0.087) and (0.146, 0.077), respectively. This is very close to the NTSC (National Television Standards Committee) blue standard (CIE: 0.14, 0.08) and the emission does almost not change over a wide range of driving voltages (Figure S8, Supporting Information). Moreover, the electro-generated emissive light from the NI-1-TPA and NI-2-TPA devices is evidently more pure than that of an analogous molecule based on PI (PI-TPA), which was reported by Ma's group in a similar device configuration and displayed CIE coordinates of (0.15, 0.11).^[8c] In addition, their CIE_y values were also smaller than that of a BI-based fluorophore (BI-TPA), which also gave CIE coordinates of (0.15, 0.11).^[15] The more 'ideal' blue-light emission from the devices based on the NI compounds might benefit from the asymmetric structures, which lead to their molecular arrangement differed from the BI and PI molecules. As expected, both the MA and MB devices showed favorable maximum CE values of 3.33 and 3.76 $cd A^{-1}$ (corresponding to EQE values of 4.12% and 5.16%), and the superior performance of the MB device could be mainly attributed to the higher PLQY of NI-2-TPA compared to that of NI-1-TPA. The devices based on NI-1-PhTPA and NI-2-PhTPA attained an amazing efficiency with EQE values of 6.08% and 5.95% (corresponding to CE values of 6.35 and 5.46 $cd A^{-1}$) and their light emission was located in the deep-blue region with CIE coordinates of (0.143, 0.115) and (0.145, 0.100), respectively.

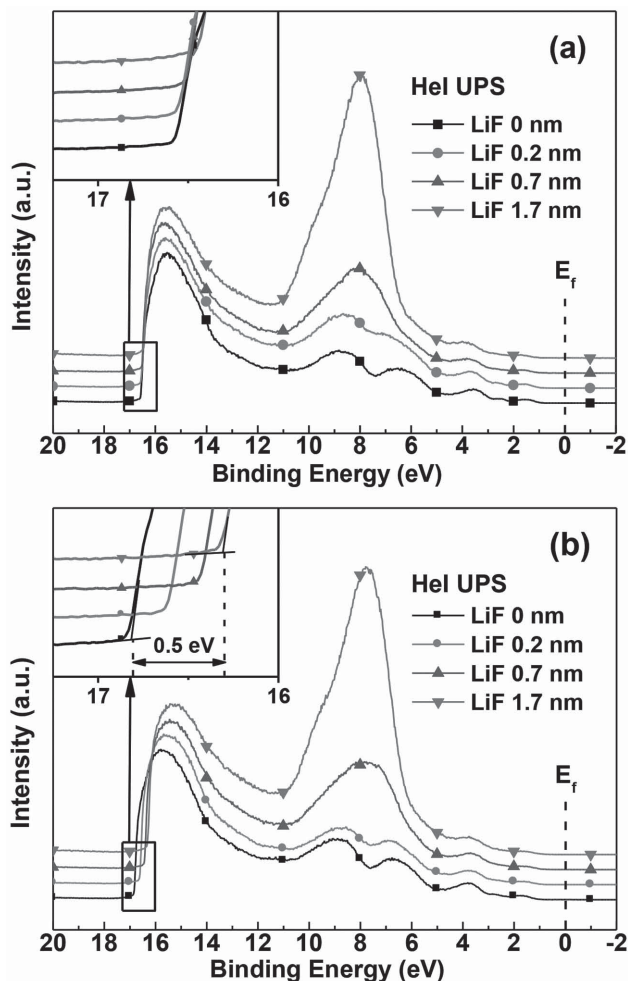


Figure 4. Hel UPS spectra obtained upon the formation of a) NI-1-PhTPA/LiF and b) NI-2-PhTPA/LiF interfaces.

From the transient PL decay curves we can deduce that the neat films of the NI compounds do not present a delayed lifetime component of emitting light (only during a short portion of the lifetime of about 2.2 ns, Figure S9, Supporting Information), showing that these emitters are totally different from TADF materials. The multi-layer devices displayed only a slight efficiency roll-off, indicating a good charge balance thanks to the felicitous D–A type molecular design. These results are among the best performances of non-doped blue-fluorescent devices and prove that both the NI-1 and NI-2 compounds may serve as excellent deep-blue emitters, whereby the latter ones exhibited an even better blue electroluminescence compared to their isomeric counterparts. We also studied the electroluminescent properties of analogous blue emitters based on BI and PI (BI-PhTPA and PI-PhTPA) with exactly the same device structure, which gave a bathochromic-shifted emission with CIE coordinates of (0.148, 0.140) and (0.151, 0.149), respectively (Figure S10, S11, and Table S3, Supporting Information). These results further prove that the current NI molecules attained an outstanding blue color purity compared to their BI and PI counterparts.

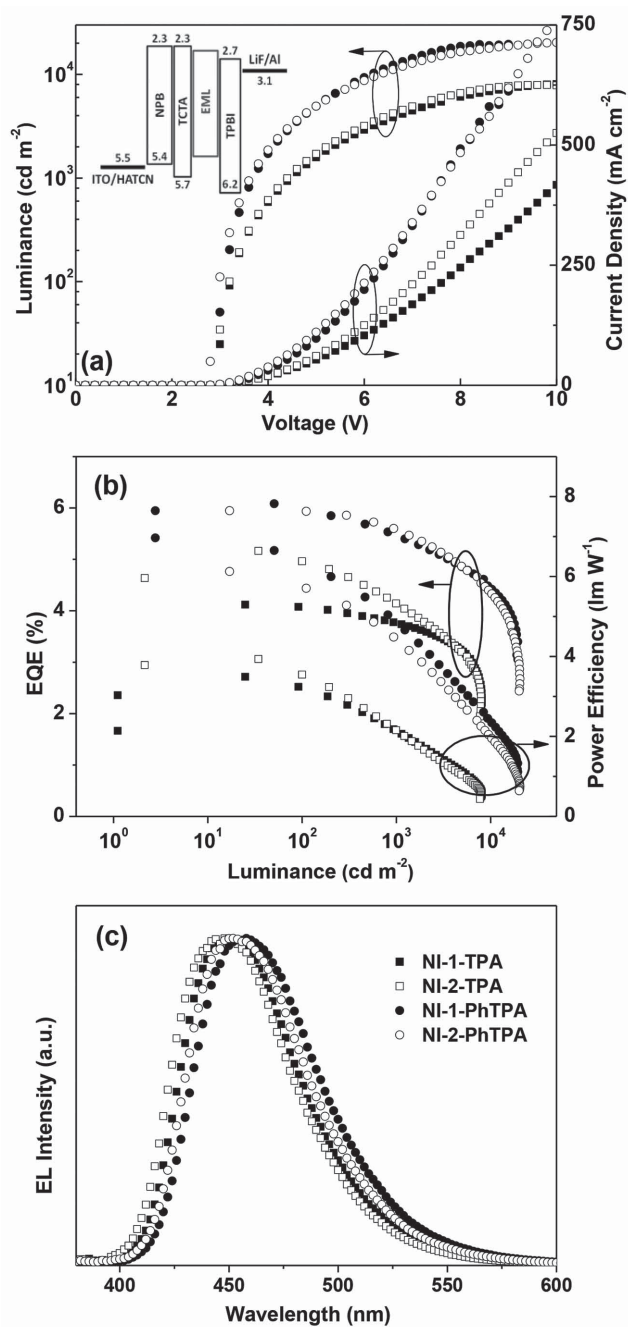


Figure 5. a) Luminance and current density versus voltage, b) EQE and PE versus luminance, and c) EL spectrum characteristics of the multi-layer devices in a structure of ITO/ HATCN (5 nm)/ NPB (40 nm)/ TCTA (5 nm)/ EML (20 nm)/ TPBI (40 nm)/ LiF (1 nm)/ Al. EML: NI-1-TPA, NI-2-TPA, NI-1-PhTPA, or NI-2-PhTPA. Inset: The configuration and energy diagram of the multi-layer devices.

3. Conclusion

A series of D–A molecules based on naphtho[1,2-*d*]imidazole isomers was synthesized and adopted as blue emitters for OLEDs. The 1*H*-naphtho[1,2-*d*]imidazole based compounds exhibited slightly blue-shifted absorption and emission spectra compared to the 3*H*-naphtho[1,2-*d*]imidazole

based ones. In addition, a remarkable efficiency with EQEs exceeding 4% was achieved for a single-layer device using a 1*H*-naphtho[1,2-*d*]imidazole based molecule, NI-2-PhTPA, as a non-doped emitting layer, whereas the 3*H*-naphtho[1,2-*d*]imidazole compounds exhibited a poor performance in single-layer devices owing to their inferior direct electron injection from the cathode. This is the best result so far for non-doped fluorescent OLEDs without additional carrier-transport materials. Introducing both hole- and electron-transporting layers to compensate for the carrier injection and to confine the carriers within the emissive layer, excellent performances with EQE values of 4.12–6.08% and deep-blue light emission with CIE_y values between 0.077 and 0.115 were obtained for both types of compound. The current findings open new avenues to designing highly efficient fluorophores for OLED applications with extraordinarily simple structures, especially for blue fluorophores, which is significant for commercial applications in flat-panel displays and lighting sources.

4. Experimental Section

General Methods: The NMR data were collected on a Bruker AVANCE Digital 600 MHz NMR workstation at room temperature. Matrix-assisted laser desorption/ionization time-of-flight (MALDI-TOF) mass spectra were recorded on a Bruker Autoflex III Smartbeam. Mass spectrometry (MS) data were obtained on a Waters TQD. Differential scanning calorimetry (DSC) measurements were performed on a Netzsch DSC 209 under N₂ flow at a heating and cooling rate of 10 °C min⁻¹. Thermogravimetric analyses (TGA) were performed on a Netzsch TG 209 under a N₂ flow at a heating rate of 10 °C min⁻¹. UV-vis absorption spectra were recorded on a HP 8453 spectrophotometer. Photoluminescence (PL) spectra were measured using a Jobin-Yvon spectrofluorometer. Cyclic voltammetry (CV) was performed on a CHI600D electrochemical workstation with a Pt working electrode and a Pt wire counter electrode at a scanning rate of 100 mV s⁻¹ against a Ag/Ag⁺ (0.1 M of AgNO₃ in acetonitrile) reference electrode in a nitrogen-saturated anhydrous acetonitrile and dichloromethane (DCM) solution of 0.1 mol L⁻¹ tetrabutylammoniumhexafluorophosphate as the electrolyte. PL quantum yields (PLQY) of the solution and film were measured by using an integrating sphere on a Hamamatsu absolute PL quantum-yield spectrometer C11347. Transient PL was measured with an Edinburgh FL920 fluorescence spectrophotometer. All reagents for synthesis were obtained from Alfa Aesar or Sigma-Aldrich and were used without further purification.

Synthesis of 1-nitronaphthalen-2-trifluoromethanesulfonate (2-1): Triethylamine was added into a solution of 1-nitro-2-naphthol (1-1, 3.8 g, 20 mmol) and 100 mL of dichloromethane. Trifluoromethanesulfonic anhydride (7.1 g, 25 mmol) was then dropped into this mixture at 0 °C. The mixture was stirred for 10 h at room temperature and was then poured into 500 mL of ice-water and extracted by dichloromethane. The combined organic phase was washed with brine and dried over anhydrous magnesium sulfate. After the solvent was removed, the product was further purified by column chromatography on silica gel to obtain a white solid (5.9 g, yield 92%). MS (ESI⁺, *m/z*): calcd. for C₁₁H₆F₃NO₅S, 321.0; found, 321.1. ¹H NMR (600 MHz, CDCl₃, δ [ppm]): 8.13 (d, *J* = 9.1 Hz, 1H), 8.01 (d, *J* = 8.2 Hz, 1H), 7.93 (d, *J* = 8.5 Hz, 1H), 7.78 (t, *J* = 7.7 Hz, 1H), 7.73 (t, *J* = 7.6 Hz, 1H), 7.57 (d, *J* = 9.1 Hz, 1H). ¹³C NMR (150 MHz, CDCl₃, δ [ppm]): 140.15, 137.92, 133.22, 132.58, 130.25, 128.68, 128.40, 125.03, 122.28, 119.06, 118.50.

Synthesis of 2-nitronaphthalen-1-trifluoromethanesulfonate (2-2): 2-2 was synthesized according to the procedure described above for the synthesis of 2-1, yielding a white solid in 88% yield. MS (ESI⁺, *m/z*): calcd. for C₁₁H₆F₃NO₅S, 321.0; found, 321.1. ¹H NMR (600 MHz, CDCl₃, δ [ppm]): 8.28 (dd, *J* = 6.4, 2.9 Hz, 1H), 8.08 (d, *J* = 9.0 Hz, 1H),

8.01–7.99 (m, 2H), 7.83–7.77 (m, 2H). ¹³C NMR (150 MHz, CDCl₃, δ [ppm]): 139.09, 138.03, 136.42, 130.49, 129.56, 129.25, 128.32, 126.59, 123.15, 120.71, 118.50.

Synthesis of 1-nitro-*N*-phenylnaphthalen-2-amine (3-1): 2-1 (4.8 g, 15 mmol), aniline (2.8 g, 30 mmol), Pd(PPh₃)₄ (230 mg, 0.2 mmol), and anhydrous potassium carbonate (4.1 g, 30 mmol) were added into 80 mL of toluene and refluxed for 24 h. Then the reaction mixture was poured into water and extracted with dichloromethane. The organic phases were combined and dried over magnesium sulfate. After the solvent was removed, the product was recrystallized from ethanol to yield a red product (3.3 g, yield 82%). MS (ESI⁺, *m/z*): calcd. for C₁₆H₁₂N₂O₂, 264.1; found, 264.0. ¹H NMR (600 MHz, CDCl₃, δ [ppm]): 9.58 (s, 1H), 8.55 (dd, *J* = 8.7, 0.6 Hz, 1H), 7.72 (d, *J* = 9.3 Hz, 1H), 7.71–7.67 (m, 1H), 7.62–7.60 (m, 1H), 7.44–7.40 (m, 2H), 7.39–7.37 (m, 1H), 7.32 (d, *J* = 9.2 Hz, 1H), 7.28–7.25 (m, 2H), 7.24 (dd, *J* = 4.8, 3.7 Hz, 1H). ¹³C NMR (150 MHz, CDCl₃, δ [ppm]): 142.24, 138.91, 135.64, 129.94, 129.80, 129.29, 128.54, 128.00, 127.73, 125.73, 124.60, 123.98, 122.81, 116.65.

Synthesis of 2-nitro-*N*-phenylnaphthalen-1-amine (3-2): 3-2 was synthesized according to the procedure described above for the synthesis of 3-1, using 2-2 as a starting material yielding an orange solid in 85% yield. MS (ESI⁺, *m/z*): calcd. for C₁₆H₁₂N₂O₂, 264.1; found, 264.0. ¹H NMR (600 MHz, CDCl₃, δ [ppm]): 9.60 (s, 1H), 8.12 (d, *J* = 9.2 Hz, 1H), 7.94 (d, *J* = 8.6 Hz, 1H), 7.80 (d, *J* = 8.2 Hz, 1H), 7.57–7.55 (m, 1H), 7.45 (d, *J* = 9.2 Hz, 1H), 7.29–7.28 (m, 1H), 7.23–7.18 (m, 2H), 7.02 (t, *J* = 7.4 Hz, 1H), 6.88 (dd, *J* = 7.7, 0.6 Hz, 2H). ¹³C NMR (150 MHz, CDCl₃, δ [ppm]): 144.02, 139.62, 136.90, 136.08, 129.74, 129.29, 128.49, 128.20, 126.57, 126.03, 123.20, 122.22, 121.12, 120.12.

Synthesis of *N*'-phenylnaphthalene-1,2-diamine (4-1): 3-1 (2.6 g, 10 mmol) was combined with anhydrous tin(II) chloride (7.6 g, 40 mmol) and 100 mL of ethanol. The mixture was refluxed for 24 h and was then poured into water and extracted with dichloromethane. The organic phases were combined and dried over magnesium sulfate. After the solvent was removed, the crude product was purified by column chromatography on silica gel to yield a white product (1.9 g, yield 81%). MS (ESI⁺, *m/z*): calcd. for C₁₆H₁₄N₂, 234.1; found, 234.0. ¹H NMR (600 MHz, CDCl₃, δ [ppm]): 7.83 (s, 1H), 7.79 (d, *J* = 8.9 Hz, 1H), 7.51–7.39 (m, 2H), 7.28 (d, *J* = 6.7 Hz, 2H), 7.19 (t, *J* = 7.6 Hz, 2H), 6.81 (s, 1H), 6.70 (d, *J* = 5.3 Hz, 2H), 5.33 (s, 1H), 4.09 (s, 2H). ¹³C NMR (150 MHz, CDCl₃, δ [ppm]): 146.02, 137.83, 132.52, 129.32, 128.50, 125.66, 125.25, 125.11, 124.06, 122.29, 120.97, 119.02, 118.93, 114.67.

Synthesis of *N*-phenylnaphthalene-1,2-diamine (4-2): 4-2 was synthesized according to the procedure as described above for the synthesis of 4-1, starting from compound 3-2, and yielding a white solid in 79% yield. MS (ESI⁺, *m/z*): calcd. for C₁₆H₁₄N₂, 234.1; found, 234.0. ¹H NMR (600 MHz, CDCl₃, δ [ppm]): 7.72 (m, 2H), 7.64 (d, *J* = 8.7 Hz, 1H), 7.34 (m, 1H), 7.23 (m, 1H), 7.14 (t, *J* = 8.2 Hz, 2H), 7.05 (d, *J* = 8.7 Hz, 1H), 6.74 (t, *J* = 7.3 Hz, 1H), 6.57 (d, *J* = 7.7 Hz, 2H), 5.26 (s, 1H), 3.87 (s, 2H). ¹³C NMR (150 MHz, CDCl₃, δ [ppm]): 146.59, 141.94, 132.86, 129.45, 128.71, 128.19, 128.01, 126.81, 122.43, 121.18, 118.35, 118.20, 117.22, 113.35.

Synthesis of 2-(4-bromophenyl)-3-phenyl-3*H*-naphtho[1,2-*d*]imidazole (NI-1-Br): To a solution of 4-bromobenzoyl chloride (2.2 g, 10 mmol) in dichloromethane (30 mL) was added slowly 4-1 (2.1 g, 9 mmol) and triethylamine (5.7 mL, 24 mmol). The reaction mixture was stirred at room temperature for 12 h. The precipitate was collected by filtration and washed with ethanol (3 × 5 mL) and dried in vacuum to give the crude product of 5-1. This solid, which could be used directly in the next step without further purification, was added into 100 mL of acetic acid. The mixture was refluxed for 24 h and then poured into 250 mL of water and extracted with dichloromethane. The organic phase was combined and dried over magnesium sulfate. After the solvent was removed, the product was further purified by column chromatography on silica gel to get a white solid (2.78 g, total yield of two steps: 76%). MS (ESI⁺, *m/z*): calcd. for C₂₃H₁₅BrN₂, 398.0; found, 398.0. ¹H NMR (600 MHz, CDCl₃, δ [ppm]): 8.78 (d, *J* = 8.2 Hz, 1H), 7.94 (d, *J* = 8.1 Hz, 1H), 7.67 (dd, *J* = 12.3, 4.9 Hz, 2H), 7.57–7.51 (m, 4H), 7.517.47 (m, 2H), 7.47–7.43 (m, 2H), 7.37–7.34 (m, 2H), 7.33 (d, *J* = 8.8 Hz, 1H). ¹³C NMR

(150 MHz, CDCl₃, δ [ppm]): 149.27, 138.51, 136.75, 133.47, 131.61, 130.82, 130.75, 130.08, 129.18, 128.96, 128.47, 127.47, 126.92, 126.72, 124.91, 124.67, 123.63, 122.10, 110.91.

Synthesis of 2-(4-bromophenyl)-1-phenyl-1H-naphtho[1,2-d]imidazole (NI-2-Br): NI-2-Br was synthesized according to the same procedure as described above for the synthesis of NI-1-Br, starting from 4-2, and yielding giving a white solid in 77% yield (two steps). MS (ESI⁺, m/z): calcd. for C₂₃H₁₅BrN₂, 398.0; found, 398.0. ¹H NMR (600 MHz, CDCl₃, δ [ppm]): 7.95 (t, $J = 7.7$ Hz, 2H), 7.75 (d, $J = 8.8$ Hz, 1H), 7.67–7.63 (m, 1H), 7.63–7.58 (m, 2H), 7.50–7.46 (m, 2H), 7.41 (m, 4H), 7.38 (m, 1H), 7.20 (m, 1H), 7.13 (d, $J = 8.5$ Hz, 1H). ¹³C NMR (150 MHz, CDCl₃, δ [ppm]): 150.30, 140.31, 138.55, 131.70, 131.48, 130.75, 130.70, 130.31, 130.02, 129.40, 129.26, 129.00, 125.69, 124.70, 124.39, 123.63, 122.06, 120.15, 119.71.

Synthesis of NI-1-TPA: A mixture of *N,N*-diphenyl-4-(4,4,5,5-tetramethyl-1,3,2-dioxaborolan-2-yl)aniline (2.3 g, 6 mmol), NI-1-Br (2.0 g, 5 mmol), 100 mg of Pd(PPh₃)₄, potassium carbonate (2.8 g, 20 mmol), THF (15 mL), toluene (30 mL), and distilled water (20 mL) was refluxed for 24 h under argon protection. Then the mixture was extracted with dichloromethane. The organic phases were combined and dried over magnesium sulfate. After the solvent was removed, the product was further purified by column chromatography on silica gel to afford a yellow powder (2.2 g, 78%). MALDI-TOF (m/z): calcd. for C₄₁H₂₉N₃, 563.24; found, 563.19. Anal. calcd. for C₄₁H₂₉N₃: C 87.36, H 5.19, N 7.45; found: C 87.52, H 5.12, N 7.31. ¹H NMR (600 MHz, CDCl₃, δ [ppm]): 8.82 (d, $J = 7.7$ Hz, 1H), 7.93 (d, $J = 7.8$ Hz, 1H), 7.66 (d, $J = 7.8$ Hz, 4H), 7.52–7.47 (m, 8H), 7.39 (d, $J = 6.8$ Hz, 2H), 7.34 (d, $J = 8.6$ Hz, 1H), 7.26–7.23 (m, 4H), 7.14–7.11 (m, 6H), 7.03 (t, $J = 6.8$ Hz, 2H). ¹³C NMR (150 MHz, CDCl₃, δ [ppm]): 150.32, 147.62, 147.58, 141.03, 138.64, 137.10, 133.86, 133.47, 130.73, 129.98, 129.77, 129.34, 128.75, 128.55, 128.44, 127.63, 127.59, 126.96, 126.60, 126.36, 124.78, 124.56, 124.32, 123.72, 123.12, 122.21, 110.96.

Synthesis of NI-2-TPA: NI-2-TPA was synthesized according to the same procedure as described above for the synthesis of NI-1-TPA, but using NI-2-Br, which yielded a yellow solid in 79% yield. MALDI-TOF (m/z): calcd. for C₄₁H₂₉N₃, 563.24; found, 563.18. Anal. calcd. for C₄₁H₂₉N₃: C 87.36, H 5.19, N 7.45; found: C 87.48, H 5.04, N 7.37. ¹H NMR (600 MHz, CDCl₃, δ [ppm]): 7.99 (d, $J = 8.8$ Hz, 1H), 7.95 (d, $J = 8.1$ Hz, 1H), 7.75 (d, $J = 8.7$ Hz, 1H), 7.67–7.57 (m, 5H), 7.55–7.51 (m, 2H), 7.51–7.47 (m, 2H), 7.47–7.42 (m, 2H), 7.39–7.36 (m, 1H), 7.28–7.23 (m, 4H), 7.21–7.19 (m, 1H), 7.15 (d, $J = 8.1$ Hz, 1H), 7.13–7.08 (m, 6H), 7.05–7.01 (m, 2H). ¹³C NMR (150 MHz, CDCl₃, δ [ppm]): 151.27, 147.62, 147.57, 140.95, 140.44, 138.92, 133.79, 131.64, 130.69, 130.20, 129.81, 129.66, 129.38, 129.31, 129.16, 128.60, 127.64, 126.20, 125.56, 124.54, 124.50, 124.19, 123.69, 123.09, 122.12, 120.18, 119.77.

Synthesis of NI-1-PhTPA: NI-1-PhTPA was synthesized according to the procedure as described above for the synthesis of NI-1-TPA by combining NI-1-Br and *N,N*-diphenyl-4'-(4,4,5,5-tetramethyl-1,3,2-dioxaborolan-2-yl)-[1,1'-biphenyl]-4-amine, giving a green-yellow solid in 79% yield. MALDI-TOF (m/z): calcd. for C₄₇H₃₃N₃, 639.27; found, 639.22. Anal. calcd. for C₄₇H₃₃N₃: C 88.23, H 5.20, N 6.57; found: C 88.14, H 5.34, N 6.39. ¹H NMR (600 MHz, CDCl₃, δ [ppm]): 8.83 (d, $J = 8.2$ Hz, 1H), 7.94 (d, $J = 8.1$ Hz, 1H), 7.70 (d, $J = 8.4$ Hz, 2H), 7.68–7.65 (m, 2H), 7.64–7.60 (m, 4H), 7.58 (d, $J = 8.4$ Hz, 2H), 7.56–7.47 (m, 6H), 7.39 (dd, $J = 5.2, 3.2$ Hz, 2H), 7.34 (d, $J = 8.8$ Hz, 1H), 7.26 (dd, $J = 11.2, 4.6$ Hz, 4H), 7.13 (d, $J = 8.5$ Hz, 6H), 7.03 (t, $J = 7.3$ Hz, 2H). ¹³C NMR (150 MHz, CDCl₃, δ [ppm]): 150.20, 147.65, 147.40, 141.11, 139.96, 138.68, 138.51, 137.13, 137.09, 134.29, 133.52, 130.75, 130.01, 129.79, 129.34, 129.08, 128.79, 128.45, 127.65, 127.61, 127.35, 127.00, 126.77, 126.63, 124.80, 124.53, 124.38, 123.83, 123.05, 122.21, 110.97.

Synthesis of NI-2-PhTPA: NI-2-PhTPA was synthesized according to the same procedure as described above for the synthesis of NI-1-TPA by combining NI-2-Br and *N,N*-diphenyl-4'-(4,4,5,5-tetramethyl-1,3,2-dioxaborolan-2-yl)-[1,1'-biphenyl]-4-amine, giving a green-yellow solid in 79% yield. MALDI-TOF (m/z): calcd. for C₄₇H₃₃N₃, 639.27; found, 639.22. Anal. calcd. for C₄₇H₃₃N₃: C 88.23, H 5.20, N 6.57; found: C 88.29, H 5.07, N 6.43. ¹H NMR (600 MHz, CDCl₃, δ [ppm]): 8.00 (d, $J = 8.7$ Hz, 1H), 7.96 (d, $J = 8.1$ Hz, 1H), 7.77 (d, $J = 8.7$ Hz, 1H), 7.68–7.59 (m, 9H),

7.57–7.52 (m, 4H), 7.52–7.47 (m, 2H), 7.40–7.37 (m, 1H), 7.30–7.25 (m, 4H), 7.22–7.19 (m, 1H), 7.17–7.11 (m, 7H), 7.06–7.01 (m, 2H). ¹³C NMR (150 MHz, CDCl₃, δ [ppm]): 151.11, 147.63, 147.38, 141.05, 140.39, 139.96, 138.87, 138.41, 134.28, 131.65, 130.72, 130.27, 129.90, 129.70, 129.41, 129.32, 129.16, 129.06, 127.64, 127.33, 126.98, 126.63, 125.62, 124.57, 124.51, 124.25, 123.82, 123.04, 122.11, 120.20, 119.76.

Device Fabrication and Characterization: The devices were fabricated by vacuum deposition of the materials at 5×10^{-4} Pa or below onto the indium tin oxide (ITO) coated glass substrates with a sheet resistance of 20 Ω per square. Before the fabrication of the devices, the NI compounds were further purified by train sublimation. All the organic layers were deposited at a rate of 1.0–2.0 $\text{\AA} \text{s}^{-1}$. The cathode was deposited with LiF (1 nm) at a deposition rate of 0.1 $\text{\AA} \text{s}^{-1}$ and then capping with Al metal (100 nm) through thermal evaporation at a rate of 4.0 $\text{\AA} \text{s}^{-1}$. The electroluminescence (EL) spectra were measured using a PR705 spectra scan spectrometer. The luminance and current density versus driving-voltage characteristics were recorded simultaneously with measuring of the Commission Internationale de L'Eclairage (CIE) coordinates by combining the spectrometer CS200 with a Keithley model 2420 programmable voltage–current source meter. All measurements were carried out at room temperature and under ambient conditions.

Ultraviolet and X-Ray Photoelectron Spectroscopy: Experiments were carried out in a Kratos AXIS UltraDL ultrahigh vacuum (UHV) surface analysis system, consisting of a multiport carousel chamber, a deposition chamber, and an analysis chamber. The base pressures in the three chambers were better than 5×10^{-9} , 2×10^{-9} , and 3×10^{-9} Torr, respectively. All organic materials were carefully sublimed twice and entirely out-gassed to ensure a good material purity and to be able to study the intrinsic behavior. The film thickness was monitored by a quartz-crystal microbalance. Prior to film deposition, the ITO-coated glass substrates were subjected to a routine cleaning process and ex situ treated by UV-ozone exposure. The organic materials, including NI-1-PhTPA, NI-2-PhTPA, and LiF were evaporated in situ in steps onto the ITO substrates from resistively heated tantalum boats in the deposition chamber at a rate of 1–2 $\text{\AA} \text{s}^{-1}$. The samples were transferred to the analysis chamber without breaking vacuum for the UPS and XPS measurements after each deposition step. The UPS measurements were carried out using an unfiltered He I (21.2 eV) gas discharge lamp to characterize the valence states and the vacuum level (VL). There was no sign of sample charging in all measurements, even when the thickness of the organic films reached several hundreds of Angstroms. A monochromatic aluminum K α source (1486.6 eV) was used in the XPS measurements to study the interfacial chemical reactions and the development of possible molecular level bending across the interface. For the collection of secondary electrons, the samples were negatively biased at 4 V. All measurements were performed at room temperature. The photoelectrons were collected by a hemispherical analyzer with a total instrumental energy resolution of 0.1 eV for the UPS measurements and 0.5 eV for the XPS measurements. In all the UPS and XPS spectra, the Fermi level (EF) is referred to as the zero binding energy (BE).

Supporting Information

Supporting Information is available from the Wiley Online Library or from the author.

Acknowledgements

M.L. and X.L.L. contributed equally to this work. The authors greatly appreciate the financial support from the Ministry of Science and Technology (2015CB655003 and 2014DFA52030), the National Natural Science Foundation of China (91233116 and 51073057), the Ministry of Education (NCET-11-0159), and the Guangdong Natural Science Foundation (S2012030006232).

Received: May 27, 2015

Revised: June 18, 2015

Published online: July 14, 2015

- [1] a) C. W. Tang, S. A. VanSlyke, *Appl. Phys. Lett.* **1987**, *51*, 913; b) J. Kido, M. Kimura, K. Nagai, *Science* **1995**, *267*, 1332; c) S. Reineke, F. Lindner, G. Schwartz, N. Seidler, K. Walzer, B. Lussem, K. Leo, *Nature* **2009**, *459*, 234.
- [2] a) H. Yersin, J. Strasser, *Coord. Chem. Rev.* **2000**, *208*, 331; b) A. Kohler, J. S. Wilson, R. H. Friend, *Adv. Mater.* **2002**, *14*, 701; c) T. Fleetham, G. J. Li, L. L. Wen, J. Li, *Adv. Mater.* **2014**, *26*, 7116; d) H. Sasabe, J. Takamatsu, T. Motoyama, S. Watanabe, G. Wagenblast, N. Langer, O. Molt, E. Fuchs, C. Lennartz, J. Kido, *Adv. Mater.* **2010**, *22*, 5003.
- [3] Q. S. Zhang, J. Li, K. Shizu, S. P. Huang, S. Hirata, H. Miyazaki, C. Adachi, *J. Am. Chem. Soc.* **2012**, *134*, 14706.
- [4] a) S. J. Su, T. Chiba, T. Takeda, J. Kido, *Adv. Mater.* **2008**, *20*, 2125; b) C. W. Lee, Y. Im, J. A. Seo, J. Y. Lee, *Chem. Commun.* **2013**, *49*, 9860; c) S. J. Su, H. Sasabe, T. Takeda, J. Kido, *Chem. Mater.* **2008**, *20*, 1691.
- [5] a) S. L. Lin, L. H. Chan, R. H. Lee, M. Y. Yen, W. J. Kuo, C. T. Chen, R. J. Jeng, *Adv. Mater.* **2008**, *20*, 3947; b) W. Y. Hung, L. C. Chi, W. J. Chen, Y. M. Chen, S. H. Chou, K. T. Wong, *J. Mater. Chem.* **2010**, *20*, 10113; c) J. Y. Hu, Y. J. Pu, F. Satoh, S. Kawata, H. Katagiri, H. Sasabe, J. Kido, *Adv. Funct. Mater.* **2014**, *24*, 2064; d) Y. C. Li, Z. H. Wang, X. L. Li, G. Z. Xie, D. C. Chen, Y. F. Wang, C. C. Lo, A. Lien, J. B. Peng, Y. Cao, S. J. Su, *Chem. Mater.* **2015**, *27*, 1100.
- [6] a) M. T. Lee, C. H. Liao, C. H. Tsai, C. H. Chen, *Adv. Mater.* **2005**, *17*, 2493; b) T. Zhang, D. Liu, Q. Wang, R. J. Wang, H. C. Ren, J. Y. Li, *J. Mater. Chem.* **2011**, *21*, 12969; c) K. Wang, F. C. Zhao, C. G. Wang, S. Y. Chen, D. Chen, H. Y. Zhang, Y. Liu, D. G. Ma, Y. Wang, *Adv. Funct. Mater.* **2013**, *23*, 2672.
- [7] a) D. C. Chen, H. Zhou, X. C. Li, M. Liu, H. Ye, S. J. Su, Y. Cao, *Org. Electron.* **2014**, *15*, 1197; b) M. Y. Lai, C. H. Chen, W. S. Huang, J. T. Lin, T. H. Ke, L. Y. Chen, M. H. Tsai, C. C. Wu, *Angew. Chem.* **2008**, *120*, 591; *Angew. Chem. Int. Ed.* **2008**, *47*, 581; c) L. Duan, J. Qiao, Y. D. Sun, D. Q. Zhang, G. F. Dong, L. D. Wang, Y. Qiu, *Adv. Opt. Mater.* **2013**, *1*, 167.
- [8] a) S. T. Zhang, W. J. Li, L. Yao, Y. Y. Pan, F. Z. Shen, R. Xiao, B. Yang, Y. G. Ma, *Chem. Commun.* **2013**, *49*, 11302; b) C. H. Chen, W. S. Huang, M. Y. Lai, W. C. Tsao, J. T. Lin, Y. H. Wu, T. H. Ke, L. Y. Chen, C. C. Wu, *Adv. Funct. Mater.* **2009**, *19*, 2661; c) W. J. Li, D. D. Liu, F. Z. Shen, D. G. Ma, Z. M. Wang, T. Feng, Y. X. Xu, B. Yang, Y. G. Ma, *Adv. Funct. Mater.* **2012**, *22*, 2797.
- [9] a) J. J. Huang, M. K. Leung, T. L. Chiu, Y. T. Chuang, P. T. Chou, Y. H. Hung, *Org. Lett.* **2014**, *16*, 5398; b) Z. M. Wang, Y. Feng, S. T. Zhang, Y. Gao, Z. Gao, Y. M. Chen, X. J. Zhang, P. Lu, B. Yang, P. Chen, Y. G. Ma, S. Y. Liu, *Phys. Chem. Chem. Phys.* **2014**, *16*, 20772.
- [10] a) W. Z. Yuan, Y. Y. Gong, S. M. Chen, X. Y. Shen, J. W. Y. Lam, P. Lu, Y. W. Lu, Z. M. Wan, R. R. Hu, N. Xie, H. S. Kwok, Y. M. Zhang, J. Z. Sun, B. Z. Tang, *Chem. Mater.* **2012**, *24*, 1518; b) W. J. Li, Y. Y. Pan, R. Xiao, Q. M. Peng, S. T. Zhang, D. G. Ma, F. Li, F. Z. Shen, Y. H. Wang, B. Yang, Y. G. Ma, *Adv. Funct. Mater.* **2014**, *24*, 1609.
- [11] M. J. Frisch, G. W. Trucks, H. B. Schlegel, G. E. Scuseria, M. A. Robb, J. R. Cheeseman, J. A. Montgomery Jr., T. Vreven, K. N. Kudin, J. C. Burant, J. M. Millam, S. S. Iyengar, J. Tomasi, V. Barone, B. Mennucci, M. Cossi, G. Scalmani, N. Rega, G. A. Petersson, H. Nakatsuji, M. Hada, M. Ehara, K. Toyota, R. Fukuda, J. Hasegawa, M. Ishida, T. Nakajima, Y. Honda, O. Kitao, H. Nakai, M. Klene, X. Li, J. E. Knox, H. P. Hratchian, J. B. Cross, V. Bakken, C. Adamo, J. Jaramillo, R. Gomperts, R. E. Stratmann, O. Yazyev, A. J. Austin, R. Cammi, C. Pomelli, J. W. Ochterski, P. Y. Ayala, K. Morokuma, G. A. Voth, P. Salvador, J. J. Dannenberg, V. G. Zakrzewski, S. Dapprich, A. D. Daniels, M. C. Strain, O. Farkas, D. K. Malick, A. D. Rabuck, K. Raghavachari, J. B. Foresman, J. V. Ortiz, Q. Cui, A. G. Baboul, S. Clifford, J. Cioslowski, B. B. Stefanov, G. Liu, A. Liashenko, P. Piskorz, I. Komaromi, R. L. Martin, D. J. Fox, T. Keith, M. A. AlLaham, C. Y. Peng, A. Nanayakkara, M. Challacombe, P. M. W. Gill, B. Johnson, W. Chen, M. W. Wong, C. Gonzalez, J. A. Pople, Gaussian 03, Revision D.01, Gaussian, Inc., Wallingford, CT **2004**.
- [12] J. Pommerehne, H. Vestweber, W. Guss, R. F. Mahrt, H. Bässler, M. Porsch, J. Daub, *Adv. Mater.* **1995**, *7*, 551.
- [13] L. Yao, S. T. Zhang, R. Wang, W. J. Li, F. Z. Shen, B. Yang, Y. G. Ma, *Angew. Chem.* **2014**, *126*, 2151; *Angew. Chem. Int. Ed.* **2014**, *53*, 2119.
- [14] Z. H. Sheng, L. Shao, J. J. Chen, W. J. Bao, F. B. Wang, X. H. Xia, *ACS Nano* **2011**, *5*, 4350.
- [15] X. H. Ouyang, X. Y. Zhang, Z. Y. Ge, *Dyes Pigments* **2014**, *103*, 39.